


Metabolomics reveals tepotinib-related mitochondrial dysfunction in MET-activating mutations-driven models

Michaela Poliaková^{1,2}, Andrea Felser³, Katarzyna Pierzchala⁴, Jean-Marc Nuoffer³, Daniel Matthias Aebersold^{1,2}, Yitzhak Zimmer^{1,2}, Nicola Zamboni⁵ and Michaela Medová^{1,2} 

1 Department of Radiation Oncology, Inselspital, Bern University Hospital, University of Bern, Switzerland

2 Department for BioMedical Research, Radiation Oncology, University of Bern, Switzerland

3 University Institute of Clinical Chemistry, Bern University Hospital, Switzerland

4 Center for Biomedical Imaging (CIBM), EPFL SB CIBM – AIT/LIFMET, Lausanne, Switzerland

5 Department of Biology, Institute of Molecular Systems Biology, Eidgenössische Technische Hochschule Zürich, Switzerland

Keywords

MET receptor tyrosine kinase; metabolism; mitochondria; non-targeted mass spectrometry; small molecule inhibitor

Correspondence

M. Medová, Department for BioMedical Research, Maurice E. Müller-Haus, E-818, Murtenstrasse 35, 3008 Bern, Switzerland
Tel: +41 31 6323565
E-mail: michaela.medova@dbmr.unibe.ch

(Received 14 August 2018, revised 27 February 2019, accepted 12 April 2019)

doi:10.1111/febs.14852

Genetic aberrations in the hepatocyte growth factor receptor tyrosine kinase MET induce oncogenic addiction in various types of human cancers, advocating MET as a viable anticancer target. Here, we report that MET signaling plays an important role in conferring a unique metabolic phenotype to cellular models expressing MET-activating mutated variants that are either sensitive or resistant toward MET small molecule inhibitors. MET phosphorylation downregulated by the specific MET inhibitor tepotinib resulted in markedly decreased viability and increased apoptosis in tepotinib-sensitive cells. Moreover, prior to the induction of MET inhibition-dependent cell death, tepotinib also led to an altered metabolic signature, characterized by a prominent reduction of metabolite ions related to amino sugar metabolism, gluconeogenesis, glycine and serine metabolism, and of numerous TCA cycle-related metabolites such as succinate, malate, and citrate. Functionally, a decrease in oxygen consumption rate, a reduced citrate synthase activity, a drop in membrane potential, and an associated misbalanced mitochondrial function were observed exclusively in MET inhibitor-sensitive cells. These data imply that interference with metabolic state can be considered an early indicator of efficient MET inhibition and particular changes reported here could be explored in the future as markers of efficacy of anti-MET therapies.

Introduction

The activation of the MET receptor tyrosine kinase (RTK) signaling by binding of its ligand, the hepatocyte growth factor (HGF), is indispensable for a variety of biological processes, including tissue homeostasis and embryonic development [1]. Although MET–HGF interaction mediates a wide range of normal cellular activities, deregulated MET signaling is strongly

associated with tumor progression and local invasion [1]. Gain-of-function alterations of the MET receptor cause its aberrant activation and lead to oncogenic consequences [2]. In numerous types of cancers, abnormal MET activity results from activating mutations, receptor overexpression, or by upregulation of HGF expression, thus creating auto- or paracrine signaling loops

Abbreviations

CASP2, caspase-2; CoA, coenzyme A; EGFR, epidermal growth factor receptor; ETC, electron transport chain; HGF, hepatocyte growth factor; METi, MET inhibition; MS, mass spectrometry; OCR, oxygen consumption rate; PCA, principal component analysis; ROS, reactive oxygen species; RTK, receptor tyrosine kinase; TCA, tricarboxylic acid; TIGAR, TP53-induced glycolysis and apoptosis regulator; TKI, tyrosine kinase inhibitor.

[3]. MET overexpression has been detected in 20–60% of various human malignancies [4] and is associated with its transcriptional activation or gene amplification. Deregulated MET is considered to be an important molecular target in cancer therapy and several MET inhibitors are currently evaluated in Phase II and/or Phase III clinical trials [5]. These compounds, effectively targeting both overexpressed receptors and most of the activating MET-mutated variants, have previously shown promising preclinical potency in inhibiting MET signaling-mediated tumor growth, tumor-associated angiogenesis, and invasion [6]. However, and despite the relative intensive characterization of action of anti-MET compounds and their impact on activation of MET-downstream signaling cascades, important aspects of MET inhibition (METi), such as a potential metabolic reprogramming in cancer cells caused by inhibition of the MET signaling, have not been assessed so far.

Metabolomics delivers in-depth information regarding metabolic changes associated with particular phenotypic traits or responses to perturbations [7]. Current metabolomic studies in oncology mainly focus on revealing biomarkers to determine diverse states of cancer [8] and the action, responsiveness, and toxicity of drugs [9], along with therapeutic resistance [10]. Emerging data show that driver genes in cancer, deregulated function of oncogenes, and genetic mutations pertaining to critical cancer regulators and pathways such as, for example, MYC, RAS, and PI3K/Akt, are associated with explicit metabolic activities [11–13]. Furthermore, metabolomic approaches have proven to be powerful tools also in the study of drug metabolism modulated by inhibition of RTKs such as the epidermal growth factor receptor (EGFR) [14].

As to metabolic effects of specific targeting of the MET receptor, it has been previously reported that METi results in significant downregulation of the TP53-induced glycolysis and apoptosis regulator (TIGAR) with subsequent depletion of intracellular NADPH levels [15], suggesting that inhibition of a MET–TIGAR–NADPH cascade may have therapeutic relevance in cancer treatment. The aim of the present study was to explore the correlation between the inhibition of the MET receptor and cellular metabolism by comparing drug responsiveness on metabolomics level in MET inhibitor-sensitive and -resistant *in vitro* models in which the MET RTK is constitutively active due to activating point mutations. Our results imply that METi selectively modulates metabolomic profile as well as oxygen consumption rate (OCR) and mitochondrial function in drug-sensitive but not in drug-resistant cells.

Results

Distinct MET-activating mutations are characterized by different metabolic profiles

Numerous preclinical studies and clinical trials are evaluating MET as a potential therapeutic target [16,17]. Detailed understanding of less documented aspects of MET targeting, such as impact on cellular metabolism or immune response, will become particularly important for their successful clinical use. In order to gain first insights into the modulation of metabolism following MET targeting, isogenic NIH3T3 mouse fibroblast cell lines stably expressing MET-activating point mutations M1268T, Y1248H, L1213V, or H1112L (denoted as ‘M1268T’, ‘Y1248H’, ‘L1213V’, and ‘H1112L’ cells, respectively) were used. These cell lines display sensitivity (M1268T and H1112L) or resistance (Y1248H and L1213V) toward distinct MET small molecule tyrosine kinase inhibitors (TKIs) including SU11274, PHA665752, or tepotinib [18,19] and thus serve as a valuable tool in studying impact of METi on various aspects of cellular fitness. Here we initially tested the effect of tepotinib [50 nM; EMD1214063 (referred to as EMD)] on the viability of these four cell lines following 2, 8, 24, 48, and 72 h of inhibitor treatment (Fig. 1A,B). We could demonstrate that tepotinib effectively decreases viability of both sensitive cell lines (Fig. 1A,B). An approximately 50% drop after 24 h and a highly significant reduction down to 80% at later time points were observed in M1268T cells, whereas METi caused about 25% decrease in viability after 48 h and 80% after 72 h in the H1112L cells (Fig. 1B). In contrast, viability of tepotinib-resistant Y1248H and L1213V cells was not affected by METi at any of the studied time points (Fig. 1A,B). As anticipated, when assessing downstream signaling of MET in all four NIH3T3 cell lines at 30 min, 2, 8, 24, 48, and 72 h upon METi (Fig. 1C), the decrease in MET activation by tepotinib in drug-sensitive cell lines M1268T and H1112L was associated with an inhibition of the activation state of MET-downstream signaling molecules Akt and Erk1/2. On the contrary, Y1248H and L1213V cell lines did not display any inhibition of enzymatic activity of MET, Akt, and Erk1/2 upon METi (Fig. 1C).

Assessment of cell death induction by caspase-3 enzymatic activity measurements recapitulated that Y1248H and L1213V cells do not undergo apoptosis upon METi (Fig. 1D). On the other hand, METi led to a significant increase in caspase-3 enzymatic activity compared to DMSO-treated controls in M1268T upon

24, 48, and 72 h and in H1112L upon 72 h of METi treatment (Fig. 1D).

To possibly associate the documented phenotypic differences between M1268T, H1112L, Y1248H, and L1213V cells upon METi to changes in metabolic states of these MET-mutated variants, their metabolomic profiling following treatment by 50 nM of tepotinib for 30 min, 2, and 8 h was performed. As at these time points the impact of METi on cell proliferation and viability is not yet apparent (Fig. 1A,D), any differences at metabolomic level should reflect either early or intermediate events occurring following METi. These processes precede secondary events resulting from late-mediated effects of MET signaling inhibition such as cell cycle changes or apoptosis. Upon metabolites extraction, non-targeted mass-spectrometry-based metabolomics measurements were conducted and the resulting data were analyzed with respect to inter- and intra-cell lines differential responses to METi. Interestingly, unexpected evident differences on the metabolic level were detected between the four isogenic cell lines already under unperturbed conditions. More specifically, as illustrated by Volcano plots in Fig. 1E, statistically significant differences ($\log_2FC > 0.5$; adj. P -value < 0.01) in the abundance of particular metabolite ions (Table S1) were identified when comparing basal metabolomes of these four isogenic cellular models. This was at a first sight a surprising finding as the NIH3T3 cell lines used in this study all ectopically express the MET receptor that differs exclusively in the nature of receptor-activating mutation [20] and their MET expression levels as well as receptor activation [as inferred from MET autophosphorylation (e.g., pMET (Tyr1234/5) status)] are very similar (Fig. 1F). At the same time, however, their signaling downstream of the receptor (e.g., activation of the PI3K and MAPK pathways) in unperturbed state seems to have different intensity (Fig. 1F). In that respect, MET M1268T and H1112L variants, for example, appear to convey a stronger stimulus to activate downstream signals such as phosphorylation of Erk1/2 as compared to the Y1248H and L1213V variants (Fig. 1F). Thus, it is plausible to speculate that this phenomenon,

which has been previously addressed by others [21,22] and lies outside of the scope of the current study, might underlie the reported differences in the basal metabolomic profiles of cell lines harboring these distinct MET-activating mutations.

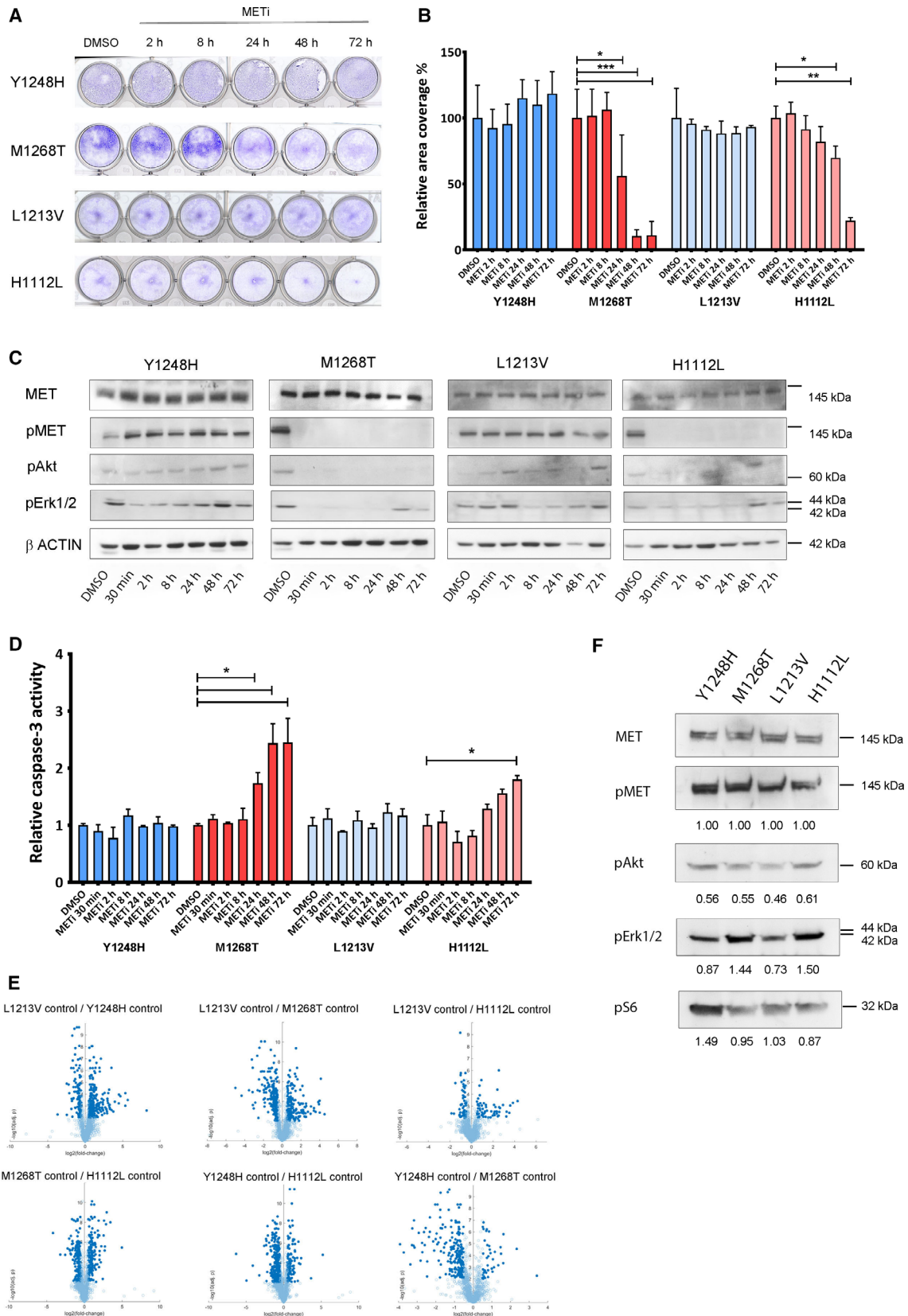
METi attenuates metabolic activity of METi-sensitive cells

To study pre-apoptotic impacts of METi on cellular metabolome in METi-sensitive and METi-resistant cellular models, M1268T, H1112L, L1213V, and Y1248H cells were treated with tepotinib (f.c. of 50 nM) for 30 min, 2, and 8 h and differential abundance of intracellular metabolites following these perturbations as compared to DMSO-treated samples was assessed [principal component analysis (PCA) shown in Fig. 2A].

Statistically significant ($\log_2FC > 0.5$; adj. P -value < 0.01) changes in metabolite ions profiles occurred in both resistant as well as sensitive cell lines at all the studied time points (e.g., 30 min, 2, and 8 h) post METi, yet with substantially higher number of hits in tepotinib-sensitive variants (Fig. 2B). Metabolism in the H1112L cell line was mostly affected after 30 min of METi treatment, while M1268T cells displayed numerous significant changes in metabolite ion abundance at all the three studied time points, suggesting that the reaction time of drug-sensitive cell lines differs depending on the particular mutation present.

Upon 8 h of treatment, METi effectively abrogates MET-related signaling in sensitive cell lines ([23] and Fig. 1C) but at the same time the cells are not committed to apoptosis yet (Fig. 1D). Importantly, at this time point almost no significantly altered metabolite ions were detected in tepotinib-resistant Y1248H and L1213V cells, whereas a profound alteration in the metabolic state was apparent in both tepotinib-sensitive cell lines. Table 1 shows metabolite ions that were the most altered in abundance [72 metabolite ions for M1268T, 24 metabolite ions for H1112L, 7 metabolite ions for L1213V, and 18 metabolite ions for Y1248H ($\log_2FC > 0.5$; adj. P -value < 0.01)] in each of the four

Fig. 1. (A) The effect of tepotinib (50 nM) on the viability of Y1248H, M1268T, L1213V, and H1112L cell lines following 2, 8, 24, 48, and 72 h of treatment assessed by crystal violet staining. (B) Quantification of the viability (crystal violet staining) of Y1248H, M1268T, L1213V, and H1112L cell lines, showing the differential impact of tepotinib. Shown is the mean \pm SD from three independent experiments ($*P < 0.05$; $**P < 0.01$; $***P < 0.001$). (C) Western blot analysis of a time course METi treatment (30 min, 2, 8, 24, 48, and 72 h) of Y1248H, M1268T, L1213V, and H1112L cells. (D) Apoptosis evaluation by caspase-3 determination. (M1268T METi 24 h $*P = 0.0588$; 48 h $*P = 0.0526$; 72 h $*P = 0.0752$; H1112L METi 72 h $*P = 0.0554$). (E) Volcano plot showing statistically significant differences (dark blue, $\log_2FC > 0.5$; adj. P -value < 0.01) by comparing the four isogenic unperturbed cellular models Y1248H, M1268T, L1213V, and H1112L. (F) Western blot analysis of unperturbed Y1248H, M1268T, L1213V, and H1112L, loading was normalized according to total MET levels.



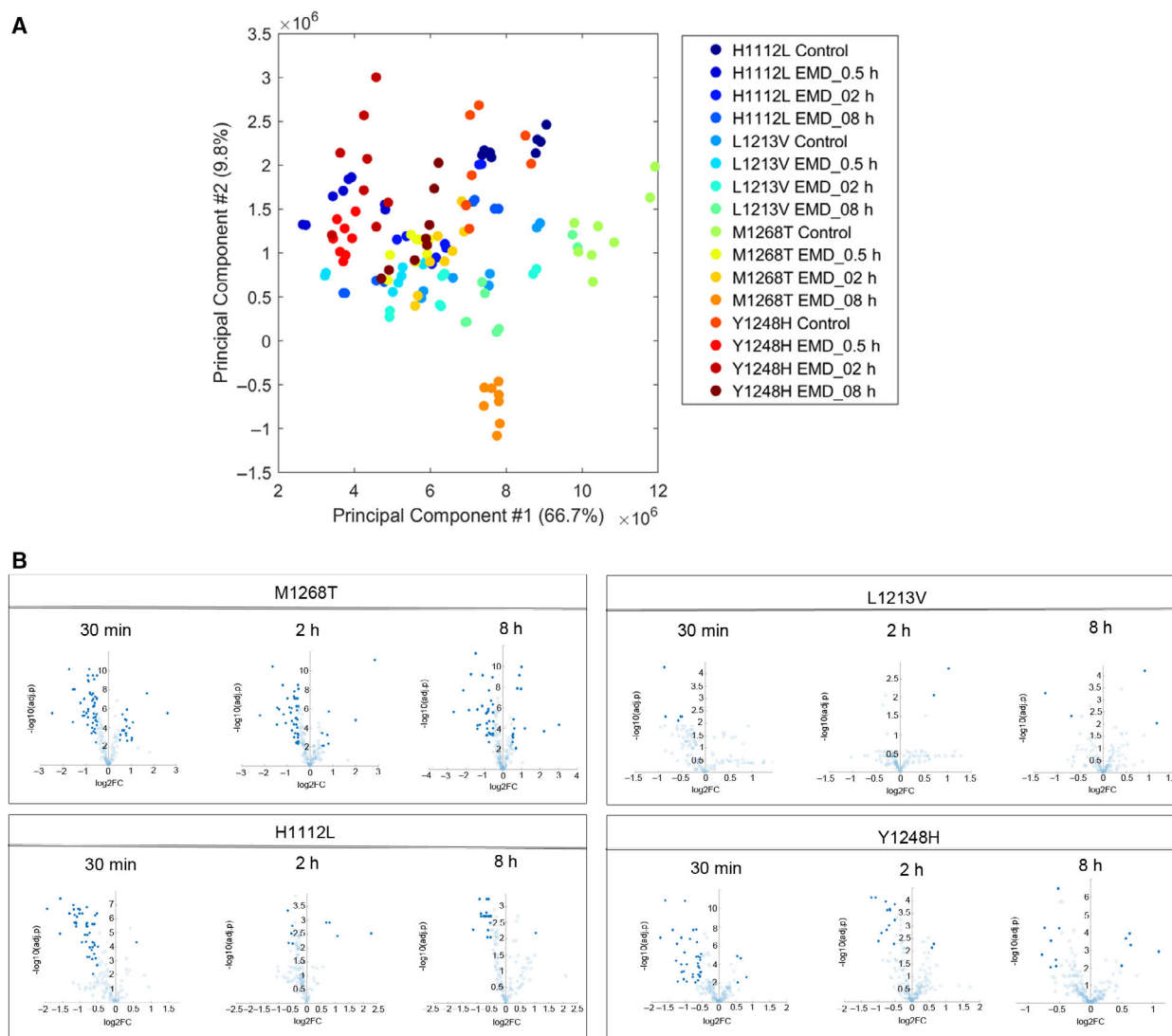


Fig. 2. (A) Principal component analysis (PCA) with two principal components. M1268T, H1112L, L1213V, and Y1248H cells were treated with tepotinib (f.c. 50 nM) for 30 min, 2, and 8 h and compared to DMSO-treated samples. (B) Volcano plots showing statistically significant differences (dark blue, $\log_2FC > 0.5$; P -value < 0.01) by comparing the perturbed (30 min; 2; 8 h METi) and unperturbed cellular models Y1248H, M1268T, L1213V, and H1112L.

cell lines following 8 h of METi by tepotinib [all altered metabolite ions in four cell lines at this time point are presented also in metabolomics networks maps (Fig. 3A)]. Interestingly, most of the metabolite ions whose occurrence was significantly changed in the Y1248H and L1213V cell lines post METi, such as for example, increased acetyl-CoA and reduced monophosphates (GMP, CMP, and UMP), tend to be altered in a similar manner also in the M1268T and H1112L cells upon tepotinib exposure, suggesting that these changes may be related to plausible off-target effects of the drug. From the METi-induced metabolic

changes that occurred after 8 h of treatment exclusively in METi-responsive cell lines, 48 out of 72 (in M1268T) and 21 out of 24 (in H1112L) [e.g., lactic acid, citric acid, lysine, pantothenic acid, pyridoxine (all affected in both these cell lines), adenylysuccinic acid, fumaric acid, malic acid, UMP/CMP/GMP, and xanthine] were decreased. This observation most likely reflects reduction in cell proliferation and a concomitant or subsequent attenuation of metabolic activity of these cells. Strikingly, these most altered metabolite ions upon METi in both drug-sensitive cells seem to be related to mitochondrial function.

Table 1. List of metabolites that were the most altered in abundance [18 metabolite ions for Y1248H, 72 metabolite ions for M1268T, 24 metabolite ions for H1112L, and 7 metabolite ions for L1213V ($\log_2FC > 0.5$; adj. *P*-value < 0.01)] in each of the four cell lines following 8 h of METi by tepotinib

Metabolite	$\log_2(FC)$	adj. <i>P</i> -value	<i>m/z</i>	<i>mz</i> difference
Y1248H METi 8 h vs Ctrl				
UMP	-1.9131068	8.55456E-05	323.0287	-0.000117374
GMP	-0.8038525	8.55456E-05	362.0509	-0.000222967
PE(16:1(9Z)/P-18:1(11Z))	0.5941949	8.55456E-05	698.5126	0.000440546
PE(18:1(11Z)/P-18:1(11Z))	0.6553709	8.55456E-05	726.5437	0.000614133
Glucosylceramide (d18:1/18:0)	0.5892093	0.000123662	726.5861	0.002814421
dUMP	-0.5594595	0.000277455	307.0343	-0.000639948
Phosphoglycerate	-0.5441018	0.000335076	184.9861	-0.00041831
CDP	-0.5629979	0.000394405	402.011	-6.39825E-05
Acetyl-CoA	1.0771395	0.000394405	808.1212	-0.002741938
IMP	-0.7703539	0.000712439	347.0398	3.64256E-05
Glutathione	-0.657551	0.001128423	306.0769	-0.000374071
Acetylglucosamine P	-0.5693985	0.00114458	300.049	-6.69226E-05
ADP	-0.5715384	0.002564304	426.0223	-0.000175224
NADPH (red)	1.0973315	0.003872648	744.0852	-0.001434993
Coenzyme A	-0.8346619	0.006714527	766.1079	4.48431E-05
dATP	-0.5882451	0.006714527	489.9921	0.001494474
Ketovaline	0.5074082	0.007321412	115.0401	6.40908E-06
Adenylsuccinic acid	-1.0334311	0.008973892	462.0676	-0.0008426
H1112L METi 8 h vs Ctrl				
Tetrahydrocortisol	-4.2368653	0.002427918	365.2349	-0.001538017
UMP	-1.3696665	0.006271289	323.0287	-0.000117374
CMP	-1.0780129	0.006721396	322.045	-0.000412609
Oxoproline	-1.0188136	0.000513597	128.0353	-1.97252E-05
Malate	-0.9087574	0.000440649	133.0143	-8.75444E-06
Acetyl-Glu	-0.7925104	0.000440649	188.0566	-0.000149859
Histidine	-0.7855465	0.001861758	154.0623	-0.000104323
CDP	-0.7448549	0.006271289	402.011	-6.39825E-05
Lactate	-0.7352988	0.004029021	89.02439	2.22823E-05
dADP	-0.6987542	0.002427918	410.0265	0.000760309
Pantothenic acid	-0.6823093	0.003540813	218.1037	-0.000271253
Pyridoxine	-0.6374692	0.003854689	168.0667	-5.05062E-05
Oxalosuccinic acid	-0.6333441	0.00220036	189.0048	-0.000769051
4-Acetamidobutanoate	-0.6294835	0.000440649	144.0665	0.000128309
(Iso)Leucine	-0.6123422	0.002427918	130.0873	8.95809E-05
Lysine	-0.5890686	0.003540813	145.0982	2.85199E-05
Valine; Betaine	-0.571566	0.003540813	116.0718	-5.67338E-05
UDP	-0.5621434	0.007435176	402.9952	-0.000311526
Tyrosine	-0.5542808	0.003540813	180.0663	0.000314756
Phenylalanine	-0.5465387	0.003540813	164.0717	1.50435E-05
Methionine	-0.5234327	0.003540813	148.044	-0.000190815
Cortexolone	0.6017827	0.009478665	345.2057	0.001455585
PE(14:0/18:2(9Z,12Z))	0.7061845	0.007435176	686.475	0.001633395
3 α ,21-Dihydroxy-5 β -pregnane-11,20-dione	0.7280276	0.005226116	347.2225	0.000312052
M1268T METi 8 h vs Ctrl				
CMP	-1.6318	1.02E-11	322.045	-0.00041
ATP	1.190145	2.46E-10	505.9884	0.000111
AMP	-1.20804	5.18E-10	346.0558	1.28E-05
ADP	-0.63237	1.41E-09	426.0223	-0.00018
UTP	1.005496	1.41E-09	482.9618	-0.00058
UMP	-2.78496	2.48E-09	323.0287	-0.00012
CTP	0.875788	1.31E-08	481.9773	-8.2E-05
4-Methyl-2-oxopentanoate	-0.80728	3.52E-08	129.0555	0.000207

Table 1. (Continued).

Metabolite	log ₂ (FC)	adj. <i>P</i> -value	<i>m/z</i>	<i>m/z</i> difference
GTP	1.1366	9.52E-08	521.9838	-0.00041
dATP	-0.67806	3.02E-07	489.9921	0.001494
Hexose P	-0.66721	3.02E-07	259.0247	-0.0023
Pyridoxine	-0.69641	3.55E-07	168.0667	-5.1E-05
Adenylsuccinic acid	-3.2362	4.22E-07	462.0676	-0.00084
GMP	-1.48596	4.83E-07	362.0509	-0.00022
Oxidized glutathione	-0.82538	4.83E-07	611.1451	-0.00037
CDP-ethanolamine	0.913766	4.83E-07	445.0535	-0.00044
Xanthine	-1.8626	7.06E-07	151.0263	-0.00019
Glutamate	-0.61216	7.33E-07	146.0459	-1.5E-05
CDP	-0.70073	9.45E-07	402.011	-6.4E-05
dADP	-0.74589	1.11E-06	410.0265	0.00076
Coenzyme A	-1.14896	1.24E-06	766.1079	4.48E-05
Lactate	-0.73737	2.21E-06	89.02439	2.23E-05
Aminobutanoic acid (ABA)	-0.64411	2.63E-06	102.0561	-9.6E-05
Pantothenic acid	-0.84682	4.28E-06	218.1037	-0.00027
5-L-Glutamyl-L-alanine	-0.68856	4.28E-06	217.0825	0.000474
Succinate	-0.57673	4.28E-06	117.0192	9.96E-05
Phenol sulfate	-0.51048	4.28E-06	172.9906	0.000786
dTDP	-0.77886	6.48E-06	401.0151	0.00058
IMP	-1.43349	1.09E-05	347.0398	3.64E-05
Hexuronate	-0.60528	1.11E-05	193.0349	0.000475
NADPH (red)	6.442422	1.7E-05	744.0852	-0.00143
Prostaglandin E2	-1.17871	1.75E-05	351.2172	0.000544
PC(15:0/P-18:1(11Z))	0.72656	1.98E-05	728.5597	0.000271
Palmitoleic acid	-0.99024	2E-05	253.2175	-0.00021
UDP	-0.5628	2E-05	402.9952	-0.00031
Malate	-1.28094	2.77E-05	133.0143	-8.8E-06
Hexonic acid	-1.39542	2.88E-05	195.0511	-9E-05
Acetylglucosamine P	-1.56774	3.58E-05	300.049	-6.7E-05
Ethanolamine phosphate	0.895803	5.84E-05	140.0119	-6.7E-05
dUMP	-0.68482	6.93E-05	307.0343	-0.00064
Hydroxyglutarate	-0.58757	7.4E-05	147.0301	-0.00019
(Iso)Citrate	-1.47429	0.000107	191.02	-0.00032
Glucosylceramide (d18:1/18:0)	0.579293	0.000109	726.5861	0.002814
Chenodeoxycholic acid	-0.84565	0.000132	391.2851	0.000263
PE(18:1(11Z)/P-18:1(11Z))	0.635625	0.000147	726.5437	0.000614
Acetyl-CoA	1.818765	0.000182	808.1212	-0.00274
Orotidine	-0.70689	0.000221	287.0523	-0.00018
Alpha-Linolenic acid	-0.53237	0.00034	277.2172	7.63E-05
Diadenosine triphosphate	-0.53016	0.00034	755.0769	-0.00221
Oxoproline	-0.52397	0.00034	128.0353	-2E-05
C22:6	-0.78572	0.000368	327.2328	9.77E-05
Inosine	-0.99563	0.000378	267.0735	-4.2E-05
Urate	-0.71789	0.000443	167.0209	0.000149
PE(16:1(9Z)/P-18:1(11Z))	0.636702	0.000644	698.5126	0.000441
Iodotyrosine	-0.51065	0.000645	305.9631	0.000189
Lysine	-0.59286	0.00069	145.0982	2.85E-05
Ketovaline	0.546207	0.000752	115.0401	6.41E-06
PE(16:0/22:6(4Z,7Z,10Z,13Z,16Z,19Z))	0.673313	0.00083	762.5091	-0.00113
C15:5	0.544101	0.000934	189.0915	0.000636
8,11,14-Eicosatrienoic acid	-0.91361	0.001013	305.2488	-0.00017
Hexose bisP	-1.04899	0.001057	338.9892	-0.0004
PC(15:0/18:2(9Z,12Z))	0.555055	0.001057	742.5391	9.96E-05
PC(15:0/20:5(5Z,8Z,11Z,14Z,17Z))	0.624708	0.002181	764.524	-0.00047

Table 1. (Continued).

Metabolite	log ₂ (FC)	adj. <i>P</i> -value	<i>m/z</i>	<i>mz</i> difference
PS(18:0/20:4(8Z,11Z,14Z,17Z))	0.599255	0.00252	810.5284	0.000702
C24 Cer	0.551675	0.002592	648.6286	0.001441
Lipoamide	-0.66136	0.002691	204.052	0.000236
Cholestane-3,7,12,25-tetrol-3-glucuronide	-0.74516	0.002859	611.3793	0.000772
PE(O-18:1(1Z)/20:4(5Z,8Z,11Z,14Z))	0.509356	0.003328	750.5445	-0.00023
PE(20:4(5Z,8Z,11Z,14Z)/P-18:1(11Z))	0.550027	0.004772	748.5276	0.001089
PE(18:3(6Z,9Z,12Z)/P-18:1(11Z))	0.57514	0.005065	722.5127	0.000277
PE(22:6(4Z,7Z,10Z,13Z,16Z,19Z)/P-18:1(11Z))	0.512614	0.005536	772.528	0.000653
PE(O-16:1(1Z)/22:6(4Z,7Z,10Z,13Z,16Z,19Z))	0.506793	0.007709	746.5116	0.001447
L1213V METi 8 h vs Ctrl				
5-Aminoimidazole ribonucleotide	-0.6339898	0.000107112	294.0471	0.002535516
4-Coumaryl alcohol	1.3672634	0.000107112	149.061	-0.00018237
N-Desmethyltamoxifen	-1.6319744	0.000371828	356.1992	0.002771699
Tetrahydrocortisol	-1.9853996	0.0016536	365.2349	-0.001538017
CMP	-0.6928528	0.0016536	322.045	-0.000412609
Prunasin	-0.7017561	0.003384613	294.0973	0.001038583
Aminobutanoic acid (ABA)	-0.7514806	0.004595023	102.0561	-9.64506E-05

Given the metabolic differences observed between untreated tepotinib-sensitive and tepotinib-resistant cells, we created heat maps (Fig. 3B) determining top hits of metabolite ions in the drug-sensitive cell lines M1268T and H1112L at the 30 min, 2, and 8 h time points post METi, which do not occur in the drug-resistant Y1248H and L1213V cells. Although these changes do not appear relevant for both tepotinib-sensitive cell lines necessarily at identical time points, many metabolite ions that are affected by METi in both M1268T and H1112L cells have the same mode of regulation (Fig. 3B). At 30 min upon tepotinib treatment, metabolite ions such as glycine, alanine, fumarate, and hexose phosphate were downregulated in both tepotinib-sensitive cells and significant at the same time at least in one of them. Similarly, UMP and lactate as well as citrate, UDP and pyridoxine metabolite ions were downregulated in tepotinib-sensitive cell lines at 2 or 8 h post METi, respectively.

METi significantly alters TCA-associated metabolism in METi-sensitive cells

Pathway enrichment analysis (Fig. 4) ($\log_2\text{FC} > 0.5$; adj. *P*-value < 0.01) revealed that the alterations observed in both M1268T and H1112L cells upon METi at time points ranging from 30 min to 8 h pertain to amino sugar metabolism (about two- to threefold decrease at 30 min and 8 h), DNA replication fork function (>5 -fold change at 30 min and 8 h), citric acid cycle (fold change of up to 5 in H1112L

30 min post METi), gluconeogenesis and glycine and serine metabolism (two- to threefold decrease upon METi), lactose synthesis (two- to fourfold change decrease at both 30 min and 8 h), and metabolites associated with transcription/translation and with transfer of acetyl groups into mitochondria (up to sixfold change decrease). Importantly, aside from the slightly altered pyrimidine metabolism and metabolites associated with transcription/translation, these pathways were not affected by tepotinib in the isogenic drug-resistant cell lines Y1248H and L1213V.

Since many of the pathways that were altered in response to METi in tepotinib-sensitive cell lines are associated with the function of mitochondria [e.g., citric acid cycle, transfer of acetyl groups into mitochondria) and also most of the metabolite ions reported in Table 1 (e.g., fumaric acid, pantothenic acid, pyridoxine, malic acid] are related to mitochondrial pathways, we focused our further analysis solely on changes of all mitochondria-relevant metabolite ions in all four cell lines at the three investigated time points (Fig. 5). A substantially higher number of changes related to mitochondria-associated metabolite ions was detected in METi-sensitive M1268T and H1112L cells compared to the drug-resistant cell lines Y1248H and L1213V. Importantly, TCA cycle metabolite ions were decreased following METi in both tepotinib-sensitive cell lines. Fumarate, malate, oxoglutarate and citrate were significantly decreased in the H1112L cell line upon 30 min of METi and partially but not significantly after 2 and 8 h of treatment. Succinate, malate, and citrate were decreased

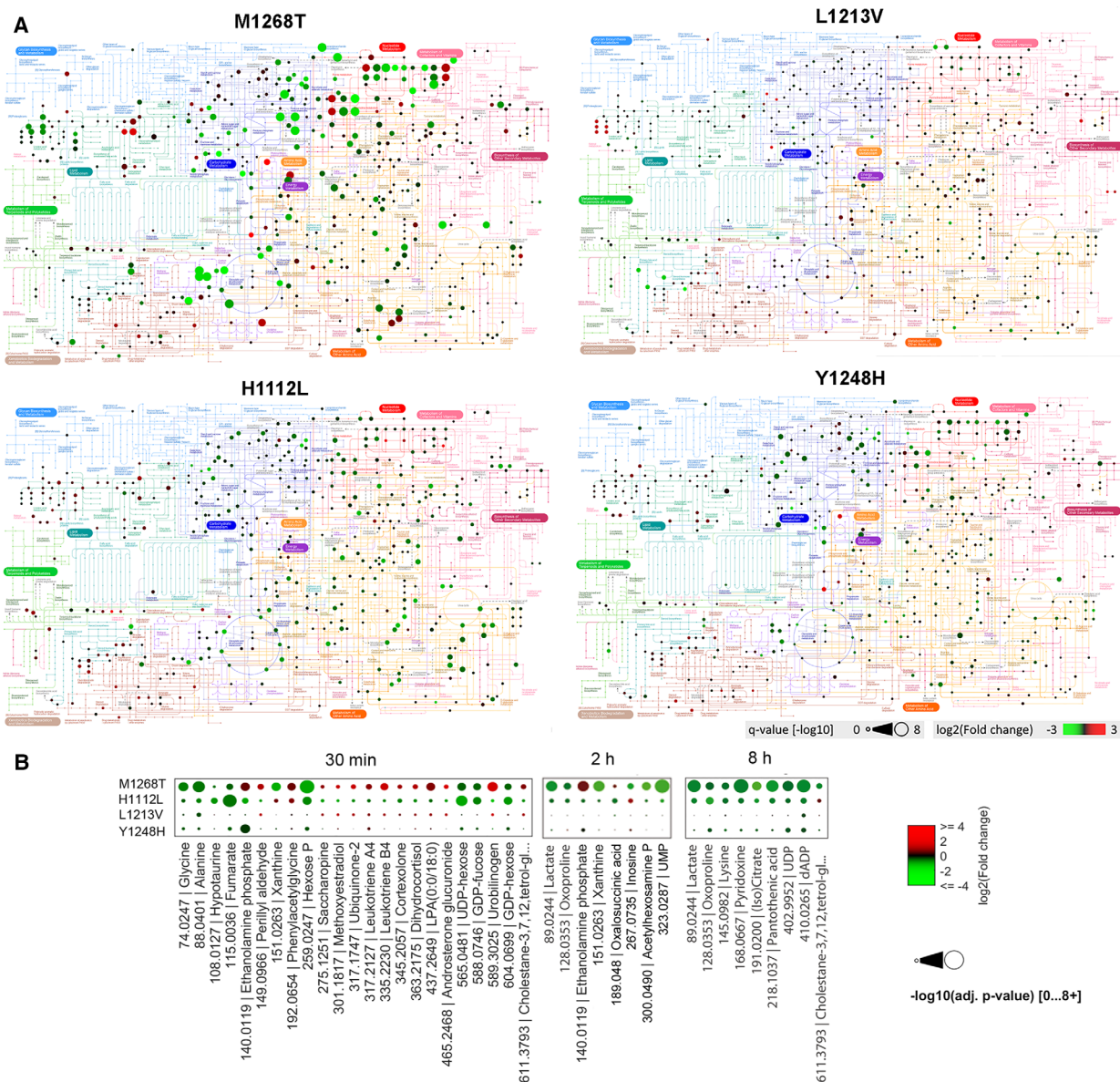


Fig. 3. (A) Metabolomic Network Maps for M1268T, H1112L, L1213V, and Y1248H cell lines, where the changed metabolite ions are plotted according to the fold change and significance upon 8 h of METi. (*Light Blue region*—Glycan Biosynthesis and Metabolism, *Cyan*—Lipid Metabolism, *Dark Blue*—Carbohydrate Metabolism, *Light Green*—Metabolism of Terpenoids and Polyketides, *Light Brown*—Xenobiotics Biodegradation and Metabolism, *Dark Orange*—Metabolism of Other Amino Acid, *Light Orange*—Amino Acid Metabolism, *Red*—Nucleotides Metabolism, *Purple*—Energy Metabolism, *Dark Pink*—Biosynthesis of Other Secondary Metabolites, *Light Pink*—Metabolism of Cofactors and Vitamins). (B) Heat map determining top hits of metabolites in the drug-sensitive cell lines M1268T and H1112L at the 30 min; 2 and 8 h timepoint post METi, without changes occurring in the drug-resistant Y1248H and L1213V cellular models.

upon METi at all given time points in both lines. The drop of nucleotide diphosphates (ADP and GDP) as well as of coenzyme A was also detected at all given time points in M1268T cells and following 30 min of METi in the H1112L cell line. Strikingly, nucleotide triphosphates (ATP and GTP) were increased in M1268T upon 8 h of METi, whereas a decrease was observed upon 30 min of METi treatment in H1112L

cells. However, levels of ADP and AMP were decreased upon METi in Y1248H, M1268T, H1112L and in Y1248H, M1268T, L1213V, respectively, (Table S2), suggesting potential off-target effects of tepotinib. Taken together, observed overall decrease in TCA-related metabolite ions in METi-sensitive cell lines indicate METi-induced changes in mitochondrial function.

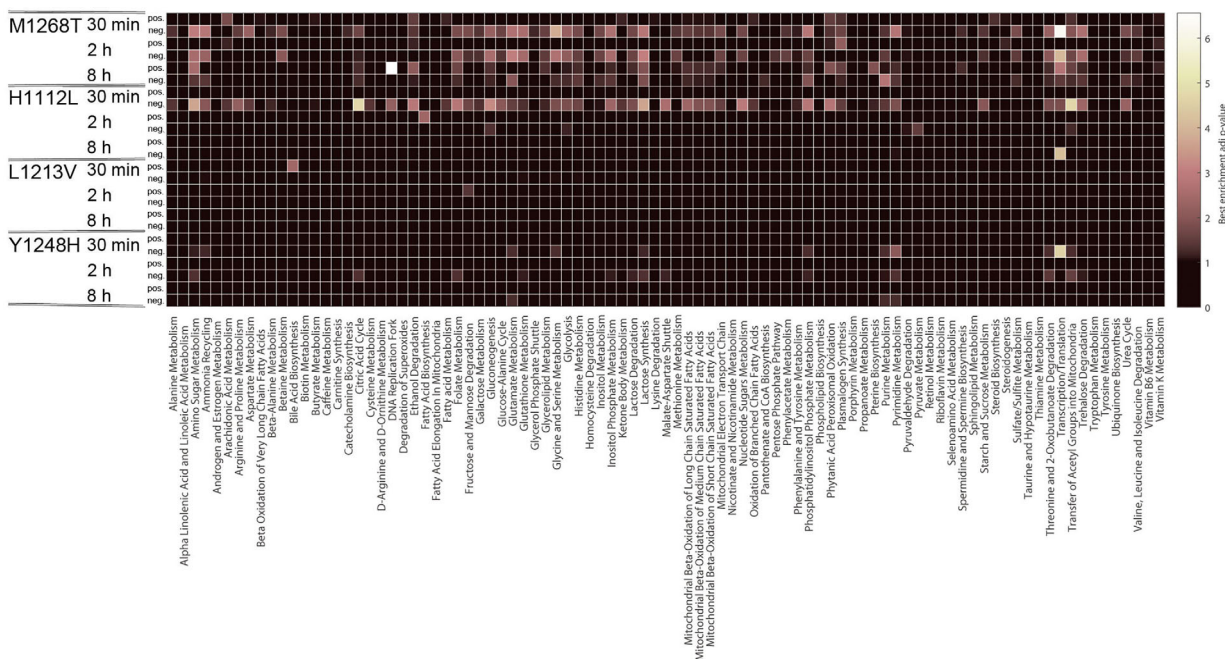


Fig. 4. Pathway enrichment analysis ($\log_2FC > 0.5$; adj. P -value < 0.01) revealing alterations observed in Y1248H, M1268T, L1213V, and H1112L cells upon METi at timepoints ranging from 30 min to 8 h (pos: positive change of pathway compared to the perturbed cell line to Ctrl; neg: negative change upon METi compared to Ctrl.)

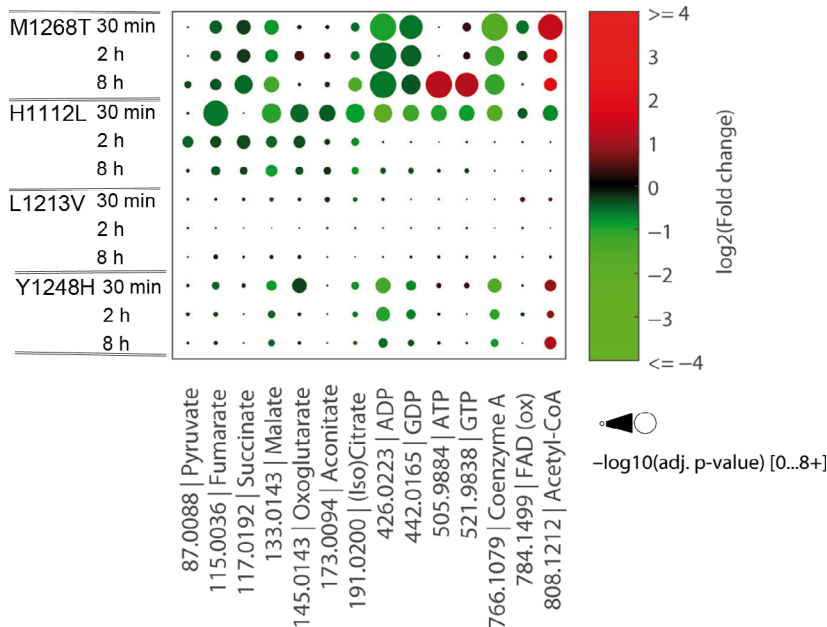


Fig. 5. Metabolic changes of all mitochondria-relevant metabolite ions in Y1248H, M1268T, L1213V, and H1112L cellular models at the 30 min; 2 and 8 h timepoint post METi.

METi affects mitochondria and its function

As on the metabolomic level, we could detect changes in abundance of numerous TCA cycle metabolite ions (Fig. 5) or metabolites associated with this pathway in both METi-sensitive cell lines M1268T and H1112L

(Table S2), we wished to further explore whether METi possibly alters cellular mitochondrial function. To that end, we investigated oxygen consumption rate (OCR) and extracellular acidification rate (ECAR) in METi-sensitive M1268T and METi-resistant Y1284H cell line. As expected, METi treatment for 8 h

decreased basal and maximal mitochondrial OCR (~ 25%) in M1268T cells, leading to a decreased ATP-derived OCR (~ 35%) (Fig. 6A,B). In contrast, basal or maximal OCR levels were not affected by tepotinib in Y1248H cells. Interestingly, we found a ~ 2-fold increased leak respiration in Y1248H cells, which led to a decrease in ATP-derived OCR (~ 25%), an observation that might be related to mild uncoupling of mitochondria [24] and potential off-target effects of tepotinib (Fig. 6A,B).

Extracellular acidification rate was not affected in any of the two investigated cell lines, suggesting that tepotinib might not directly interfere with cellular glycolytic rates. Interestingly, Y1284H cell line substantially decreased ECAR in response to the respiratory chain inhibitors rotenone and antimycin A (~ 70%), while ECAR was only marginally decreased in M1268T (~ 25%) under the same conditions (Fig. 6C-D). These findings indicate that aerobic CO₂ contributions to ECAR are different in these two isogenic cell lines [25].

Moreover, the activity of citrate synthase, a commonly used marker of mitochondrial abundance [26], was significantly reduced following METi in M1268T but not in Y1248H cells as compared to their untreated controls (Fig. 6E). Interestingly, basal expression of citrate synthase seems to be significantly higher (by ~ 40%) in M1268T cells as compared to the Y1248H line (Fig. 6E), an observation that could be potentially attributed to different metabolic profiles of these isogenic cell lines (Fig. 1C).

We further examined mitochondrial status of these cells following METi by visualizing this cellular compartment using MitoTracker[®] that is taken up by and concentrated in metabolically active mitochondria. Interestingly, mitochondria in METi-treated M1268T cells show granular appearance with expression of brighter fluorescence, whereas mitochondria in Y1248H cells do not change its phenotype upon

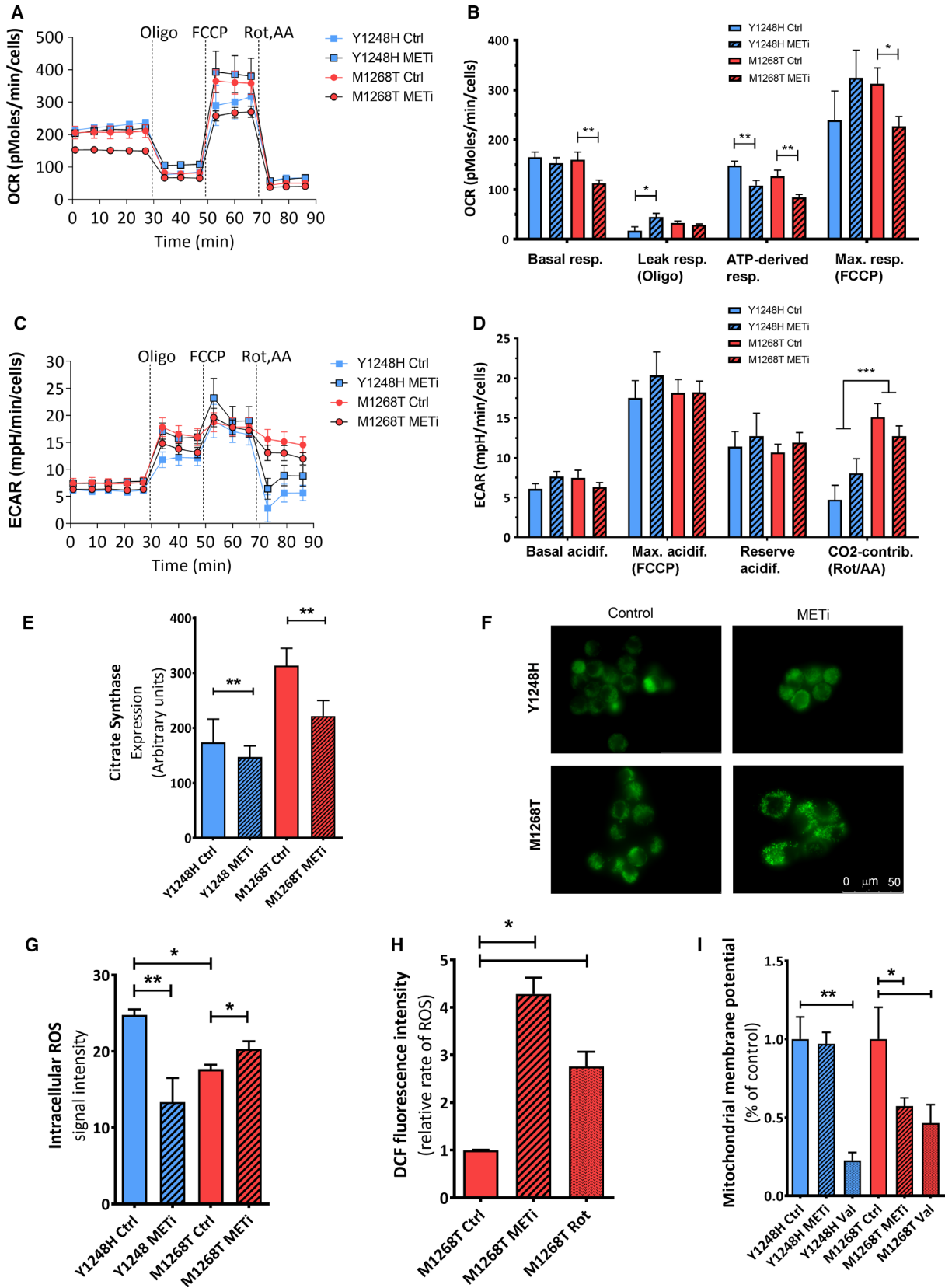
tepotinib treatment (Fig. 6F). As mitochondria are an important source of reactive oxygen species (ROS), its production subsidizes to mitochondrial damage and furthermore is crucial in redox signaling within the cell [27]. Elevated ROS activity (by ~ 25%) was detected in Y1248H control cells in comparison to M1268T control. Although we observed inhibition of ROS production in Y1248H cells exposed for 8 h to METi, in the drug-sensitive M1268T mutants, ROS production upon METi for 8 h appears to be significantly increased by ~ 15% (Fig. 6G). This METi-stimulated induction of ROS in M1268T cells was also confirmed by the use of the cell-permeant 2',7'-dichlorodihydrofluorescein diacetate (H₂DCFDA) (Fig. 6H). Tepotinib reduced the mitochondrial membrane potential ($\Delta\psi$) by 30% in tepotinib-sensitive M1268T cells; however, no change was observed in the tepotinib-resistant cell line (Fig. 6I). Importantly, this finding can be potentially correlated with METi-induced changes in mitochondrial morphology.

Discussion

The proto-oncogene MET controls genetic programs leading to proliferation, invasiveness and anti-apoptotic behavior. In the present study, we examined the impact of selective inhibition of MET signaling by the potent small molecule inhibitor tepotinib [28] in MET-mutated NIH3T3 fibroblasts and report for the first time that already a short treatment by METi considerably modulates cellular metabolism and impairs mitochondrial function. We hypothesize that these events precede and eventually contribute to cell death, the ultimate fate of these cells induced by prolonged METi.

To study metabolic responses toward METi, we have employed four isogenic cellular systems differing solely in the nature of MET-activating mutation, two

Fig. 6. (A) Timelines of cellular OCR under basal condition and after addition of modulators of mitochondrial function in both cell lines, comparing control and METi treatment for 8 h. (B) Quantification of OCR steady-state levels of basal (M1268T METi 8 h **P* = 0.012), leak (Y1248H METi 8 h **P* = 0.02), ATP-derived (M1268T METi 8 h ***P* = 0.005; Y1248H METi 8 h ***P* = 0.007), and maximal respiration (M1268T METi 8 h **P* = 0.03). (C) Timelines of cellular ECAR under basal condition and after addition of modulators of mitochondrial function in both cell lines, comparing control and METi treatment for 8 h. (D) Quantification of ECAR steady-state levels of basal, maximal, reserve, and aerobic CO₂-contributed acidification (Y1248H:M1268T ****P* = 0.00003). (E) Quantification of citrate synthase activity for both cell lines, treated with METi for 8 h (M1268T METi 8 h ***P* = 0.0045; Y1248H:M1268T ****P* = 0.0017). CS activity is normalized to the total protein content of the sample used in the assay. (F) Effect of METi for 8 h on mitochondria followed by MitoTrackerGreen[®] in both cellular models. (G) Intracellular ROS generation rate for both cell lines (controls and tepotinib-treated) calculated from ESR kinetic plots (EPR signal levels versus the elapsed time; Y1248H:M1268T **P* = 0.018; M1268T METi 8 h **P* = 0.007; Y1248H METi 8 h ***P* = 0.004). (H) ROS assessment by DCFDA in M1268T cells (M1268T METi 8 h **P* = 0.0109; M1268T Rot **P* = 0.0879). Data are presented as means ± SEM (**P* < 0.05; ***P* < 0.01; ****P* < 0.001). (I) Effect of tepotinib and valinomycin on membrane potential ($\Delta\psi$) in Y1248H and M1268T (M1268T METi 8 h **P* = 0.049; M1268T Val **P* = 0.0825; Y1248H Val ***P* = 0.0056).



mutants being sensitive while two others resistant toward MET targeting [20]. Unexpectedly, distinct basal metabolomic profiles were observed in these mutants, most likely related to their differential engagement with regard to MET-downstream signaling. In this respect, it has been previously reported that signal transduction induced by different activating MET mutations can lead to preferential stimulation of distinct signaling pathways downstream of the receptor [22]. Specifically, particular MET mutations such as M1250T and D1228H hyperactivate the RAS signaling pathway, whereas other (e.g., L1195V and Y1230C) predominantly interact with the intracellular transducer PI3K [21]. It is thus very plausible to reason that these distinct biological properties elicited by the different mutants alter their metabolic profiles.

When assessing the effect of METi on cellular metabolome in METi-sensitive systems, we detected a pronounced impact on mitochondria-related metabolite ions. In this respect, one of the most interesting observations originating from metabolomics profiling of MET mutant-expressing cellular systems upon METi (Fig. 2B and Table 1) is the deregulation of the levels of distinct vitamins such as pantothenic acid (B5) and pyridoxal (B6) in the METi-sensitive cell lines M1268T and H1112L following METi for 8 h. In view of the fact that METi seems to interfere with mitochondrial function, it is interesting to note that the biosynthesis of the component of mitochondrial respiratory chain, coenzyme Q, is dependent on these particular vitamins [29]. Moreover, pantothenic acid is a precursor of coenzyme A (CoA) which functions as an essential acyl group carrier and carbonyl-activating group in mitochondria. However, a plausible direct association between the drop in levels of certain vitamins and mitochondrial stage upon MET targeting would need to be further explored.

METi-induced reduction of other mitochondria-related metabolite ions reported by our study, such as succinate, fumarate, malate, and citrate, suggests a blockage of the TCA cycle, which produces reducing equivalents FADH₂ and NADH that fuel the electron transport chain (ETC) with their electrons [30]. Moreover, lactate, which was decreased upon METi in tepotinib-sensitive cells, was shown to be a primary source of carbon for the TCA cycle and thus of energy [31] and it was suggested, that lactate can act as a fuel for tumors [32]. Interestingly, additional secondary activity metabolite ions related to the mitochondrial function such as hydroxyglutarate, lysine and lactate were decreased after blockade of MET signaling, suggesting that METi treatment causes mitochondrial dysfunction. Hydroxyglutarate is converted from oxoglutarate,

a major intermediate in citric acid cycle, by phosphoglycerate dehydrogenase [33] and lysine was reported to have a role in mitochondrial function and damage [34]. Lactate is on the other hand used by mitochondria as a carbon source to respire [35]. Supporting our findings, Lanning *et al.* [36] recently reported that the TCA cycle metabolite 2-oxoglutaric acid, a precursor of glutamate, was significantly reduced upon treatment with the selective MET inhibitor capmatinib in two TNBC mesenchymal-like cell lines MDA-MB-231 and Hs578. Similarly, TCA cycle and central carbon metabolites such as aspartate, fumarate, and malate were decreased as well following erlotinib treatment [36].

Altogether, our current data suggest a role of mitochondrial dysfunction as a potential factor at the origin of the reduction of mitochondrial metabolites by cancer cells with deregulated MET activity consecutive to treatment with tepotinib. It is generally accepted that fundamental mitochondrial functions are to participate in calcium homeostasis, to generate ATP for proper functioning of the cell, and to regulate the ROS [37]. We showed that OCR, an indicator of oxidative phosphorylation, was suppressed following METi in METi-sensitive M1268T cells. This observation is in line with previously reported modulations of cellular metabolism by EGFR signaling, where Makinoshima *et al.* documented changes in OCR in EGFR-inhibitor-treated lung adenocarcinoma cell line HCC827 and similar result was recapitulated by Chen *et al.* in myeloma cells treated with the specific EGFR inhibitor gefitinib [38,39]. The OCR drop in M1268T cells might be caused by impairment of mitochondrial function via mitochondrial membrane depolarization following tepotinib administration, which was previously reported using other tyrosine kinase inhibitors. Lapatinib, a dual HER2 and EGFR inhibitor, as well as gefitinib both induced cytotoxic effect and mitochondrial membrane depolarization, while sorafenib, a VEGFR, PDGFR, and RAF kinases inhibitor, promoted apoptosis and dissipation of mitochondrial potential in breast cancer cell lines [40]. The associated morphology of mitochondria after treatment with tepotinib in drug-sensitive cell line, which demonstrated a granular appearance [41], potentially indicates either (a) activation of intrinsic apoptotic pathway, where formation of short, round mitochondria is specific for apoptosis [42], thus suggesting the role of tepotinib in a regulation of mitochondria-mediated cell death, supported by finding that mitochondria is a potential direct target of MET inhibitor PHA-665752 in gastric cancer cell line SNU5 [43]; or (b) alternatively suggests a

deregulation of mitochondrial networks by METi. Intact mitochondria perform active exchange of mitochondrial DNA and proteins through mutual interactions and these networks might be disturbed by fission to fusion dysbalance [44].

We further showed that the observed change in mitochondrial morphology of M1268T cells following 8 h of METi treatment is correlated with a significant increase in ROS production. ROS production is usually stimulated by dysfunctional mitochondrial oxidative phosphorylation and causes a release of cytochrome c from mitochondria, triggering the caspase pathways and subsequent activation of apoptosis. Moreover, both endoplasmic reticulum and Ca^{2+} channels are affected by ROS and it has been shown that increased intracellular Ca^{2+} levels trigger depolarization of mitochondrial membrane, loss of membrane potential, and generation of ROS, resulting in cellular necrosis [45]. Interestingly, it has been shown that the inactivation of TCA cycle leads to an increased ROS release to the cytosol through the detoxifying capacity of mitochondria [46]. Furthermore, the elevated levels of ROS in METi-treated M1268T cell line are supported by a study showing that BRAF inhibition with vemurafenib induces an increase of oxidative stress in melanoma cancer cells by upregulating ROS concomitantly with the induction of pyruvate dehydrogenase phosphorylation [47]. The levels of ROS-scavenging enzymes such as superoxide dismutase, glutathione peroxidase, and peroxiredoxin are significantly altered in malignant cells and the difference between M1268T and Y1248H ROS levels suggests highest resistance of Y1248H to oxidative insult. We hypothesize that the observed decrease in ROS production in METi-resistant Y1248H exposed to METi for 8 h could correspond to the aberrant regulation of redox homeostasis; the redox adaptation through the elevation of endogenous antioxidants might be crucial not only in cancer development but also in the activation of cell survival pathways, capacity to tolerate exogenous stress and drug resistance [48]. Moreover, it has been reported that increased proton leak states, that are observed in Y1248H upon METi, are also associated with decreased ROS levels, possibly playing a protective role by mitigating ROS production [49].

Activity of citrate synthase, an enzyme that is allosterically regulated by several key metabolites (e.g., acetyl-CoA, ATP, citrate and succinate [50]), was decreased in M1268T cells after 8 h of METi treatment. Citrate plays a critical role in the fatty acid synthesis, where it can be used in the production of acetyl groups [51], consequently suggesting that fatty acid

synthesis can be a potential target of METi. The TCA cycle and ETC have a balanced partnership—they each lean on the other to function properly and a reduction of citrate synthase can potentially affect the flow of cellular respiration followed by tumor growth attenuation, inhibition of invasion, migration and upregulation of glycolysis in MET-overexpressing tumors as was shown previously in ovarian carcinoma with increased citrate synthase activity [52]. Interestingly, the activity of citrate synthase was higher in unperturbed Y1248H compared to M1268T, indicating that there is a difference in mitochondrial abundance between the two cell lines, most possibly caused by different metabolic profiles of these isogenic cell lines and their different intensity of downstream signals (Fig. 1D,E). A 2007 study by Sharma *et al.* [53] revealed that citrate synthase activity falls significantly under conditions of oxidative stress. Decreased citrate synthase activity was reported also in a rat brain tumor where lipid peroxidation occurred, suggesting that conditions of oxidative stress could inactivate citrate synthase [54]. Here we report a correlation between a loss of citrate synthase expression and ROS generation. Untreated M1268T cells, with comparably low ROS levels detected, displayed higher citrate synthase activity while in case of Y1248H control cells, higher ROS level, and lower citrate synthase activity were recorded, thus leading to the hypothesis that decreased citrate synthase activity may reflect oxidative inactivation.

The observed decrease in mitochondrial membrane potential can be caused by impairment of the function and/or uncoupling of the respiratory chain [55]. This reduction was compatible with impaired mitochondrial function, confirmed by decreased OCR, TCA cycle, and increased ROS levels. The decrease of mitochondrial membrane potential was shown as well in the human hepatocellular carcinoma cell line HepG2 upon treatment with imatinib, lapatinib, and sunitinib [56]. Moreover, the dysfunctions of the respiratory chain components, lower $\Delta\Psi$ and decreased activity of the respiratory chain was reported with a simultaneous increase in ROS production [57,58].

In conclusion, we report particular metabolic profiles and changes as novel readouts of MET RTK signaling and its targeting. In this respect, in response to the specific MET small molecule inhibitor tepotinib, drug-sensitive cell lines showed reduction of TCA cycle-related metabolites, decrease of OCR as well as reduction of mitochondrial metabolites and the impairment of the function of mitochondria itself, whereas no such impact of METi was observed in METi-resistant cell lines. Although further biological

investigations are warranted to understand the exact metabolic effects related to METi in MET-deregulated systems, these and similar observations could potentially serve as means to predict the response to and, more importantly, efficacy of METi treatment.

Materials and methods

Cell culture

NIH3T3 cell lines that stably express the M1268T, Y1248H, L1213V, and H1112L MET-activating point mutations (referred to as NIH3T3 MET M1268T, NIH3T3 MET Y1248H, NIH3T3 MET L1213V, and NIH3T3 MET H1112L, respectively) were previously described and their identities were documented by sequencing of both strands of DNA in the region of interest [20]. They were kindly provided by Dr. Laura Schmidt (National Cancer Institute, Frederick, MD) and maintained in DMEM (GIBCO) supplemented with 10% FCS, antibiotic-antimycotic, and 0.5 mg·mL⁻¹ Geneticin/G-418 sulfate (GIBCO, Basel, Switzerland).

MET inhibition

MET enzymatic activity was inhibited by the MET tyrosine kinase small molecule inhibitor tepotinib [EMD1214063 (referred to as EMD); Merck, Darmstadt, Germany] at a final concentration of 50 nM for the indicated time points.

Crystal violet assay

For determining viability of cultured cells upon stimulation with tepotinib, crystal violet assay was performed. A total of 4×10^4 cells per well was seeded into a 24-well plate for 24 h and afterwards, cells were allowed to grow for 72 h with tepotinib added for 72, 48, 24, 8, or 2 h before staining (controls were treated with DMSO for 24 h). Cells were subsequently fixed and stained with 2% crystal violet in 1 : 3 methanol and 2 : 3 acetic acid (v : v) for 30 min at room temperature. Stained cells were washed with deionized water until a clear background was visible. Wells were scored and quantified using the 'Analyze Particles' plug-in of ImageJ (imagej.nih.gov/ij/). Experiments were performed independently three times.

Protein extraction and western blot analysis

Cells (6 cm plates, 80% confluency) were lysed in urea lysis buffer (HEPES, urea, sodium orthovanadate, sodium pyrophosphate, β -glycerol-phosphate) followed by sonication. Total protein concentrations were determined with the Bio-Rad protein quantification reagent (Bio-Rad Laboratories, Inc., Hercules, CA, USA) and 50 μ g of total proteins were resolved by SDS/PAGE on 10% gel (50V, 3–4 h).

Separated proteins were transferred to PVDF membranes (100V, 1 h) followed by blocking with 5% milk in TBS/T for 1 h and overnight incubation with primary antibodies against p-Y1234/Y1235 MET, p-Ser473 Akt, p-Thr202/Tyr204 Erk1/2, p-Ser235/236 (Cell Signaling Technology, Danvers, MA, USA, 1 : 200 to 1 : 1000) at 4 °C. Incubation of membranes was done with appropriate secondary antibodies (1 : 1000) for 1 h at RT and signals were detected with the ECL kit (AmershamPharmacia Biotech, Little Chalfont, UK). Experiments were performed independently three times.

Apoptosis assay

Enzymatic activity of caspase-3 was evaluated via a fluorogenic assay based on the caspase-3-specific substrate Ac-DEVD-AMC (Calbiochem, San Diego, CA, USA). Cell lines were plated in 10 cm plates; the substrate was added to cell lysates after 30 min, 2, 8, 24, 48, and 72 h of treatment with tepotinib. Fluorescence was measured at excitation and emission wavelengths of 380 and 460 nm, respectively, with an Infinite 200 plate reader (Tecan Group Ltd., Männedorf, Switzerland). Caspase-3 activity was normalized to protein content and results shown are representative of at least three independent experiments.

Metabolites extraction

NIH3T3 MET M1268T, H1112L, L1213V, and Y1248H cells were seeded in six-well plates (each experimental condition was plated in quadruplicates) and treated as indicated. At every given time point, cells were washed with 75 mM ammonium carbonate (Sigma) pH 7.4, quenched by snap freezing with liquid nitrogen, and stored at -80 °C. Metabolites were extracted with 400 μ L of the extraction solution (2 : 2 : 1 acetonitrile : methanol : water; -20 °C) on ice for 10 min. The plate was re-extracted one more time with 400 μ L extraction solution, allowing for a high recovery rate to perform qualitative comparison between conditions. The extracts were collected in a 1.5 mL eppendorf tubes and centrifuged (4° C, 15 700 g, 2 min). Supernatants were stored at -20°C until analysis by mass spectrometry.

Non-targeted mass spectrometry (MS) measurements

For non-targeted metabolite profiling, samples were analyzed by flow injection analysis on a 6550 Agilent Q-TOF instrument as previously described [59], in negative ionization mode (m/z range of 50–1000) at 4 GHz high resolution mode. Ions were putatively annotated based on accurate mass against the KEGG database with a tolerance of 0.001 Da. Ion annotation matches are reported in Table S2. Statistical analysis of the resulting metabolomics data was performed using Matlab.

Extracellular flux analysis

Extracellular flux analysis was assessed in intact cells using an XF24 analyzer (Seahorse Bioscience, North Billerica, MA, USA). Oxygen consumption rate (OCR), an indicator of mitochondrial respiration, and extracellular acidification rate (ECAR), an indicator of glycolytic lactate or respiratory CO₂ production, were measured in parallel. Cells were plated into the XF24 cell culture plates (Seahorse Bioscience) at a density of 20 000 cells per well in DMEM (10% FBS) and incubated at 37 °C, 5% CO₂ overnight. Cells were treated with tepotinib for 8 h. Before the experiment, cells were washed with assay medium (unbuffered DMEM) and placed at 37 °C in a CO₂-free incubator for 1 h. OCR and ECAR of intact cells were monitored in assay medium over time under basal condition, and after addition of modulators of mitochondrial function. First the ATP-synthase inhibitor oligomycin (oligo, 1 μM) was injected to measure proton leak respiration, followed by the uncoupling agent carbonyl cyanide-*p*-trifluoromethoxyphenylhydrazone (FCCP, 1.5 μM) to stimulate respiration maximally, and finally the complex I and III inhibitors rotenone (1 μM) and antimycin A (1 μM) were added to assess non-mitochondrial respiration. After each experiment cell numbers were corrected for amount of protein in each well. OCR steady-states were calculated after subtraction of non-mitochondrial respiration. ATP-derived respiration represents the difference between basal OCR and proton leak OCR after oligomycin. Reserve acidification represents the difference between basal ECAR and maximal ECAR under FCCP.

Determination of citrate synthase activity

The mitochondrial matrix marker enzyme citrate synthase was measured spectrophotometrically using a UV-1601 spectrophotometer (Shimadzu) following the method based on Shepherd and Garland [60]. Cell homogenate was prepared in buffer containing 20 mM Tris/HCl (pH 7.2), 250 μM saccharose, 40 mM KCl, 2 mM EGTA, 1 mg·mL⁻¹ BSA, and was sonicated 3× prior to use. The reaction was conducted in assay buffer containing 100 mM Tris/HCl (pH 8), 0.2% (vol/vol) Triton X-100, 100 μM DTNB and 400 μM Acetyl-CoA using 1 mL sample cuvettes thermostatically maintained at 30 °C. The reduction of 5,5'-dithio-bis-(2-nitrobenzoic acid) (DTNB) was monitored at 412 nm and after 2 min 500 μM oxaloacetic acid was added. Values were estimated by the difference in activity levels measured in the presence or absence of oxaloacetic acid. The activity was normalized to the amount of protein in each sample.

Fluorescence light microscopy

A total of 10⁴ cells were plated on chamber slides in duplicates, treated with tepotinib for 8 h and stained with

200 nM MitoTrackerGreen[®] (Cell Signaling Technology, #9074) for 30 min. Images were acquired with a fluorescent microscope (Leica DM5500 B, 100× oil immersion phase contrast objective).

Reactive oxygen species (ROS) measurements

Cells were grown in 175 cm² tissue culture flasks (Eppendorf, Hamburg, Germany) at 37 °C, 5% CO₂ overnight. Cells were scraped (Sarstedt, Nümbrecht, Germany), centrifuged at 400 *g* for 2 min and transferred into the 2 mL Eppendorf tube with whole medium with added 10 mM 1-Hydroxy-3-methoxycarbonyl-2,2,5,5-tetramethylpyrrolidine (CMH) spin trap (Noxygen Science Transfer & Diagnostics GmbH, Lindenmatte, Germany) and incubated at 37 °C. Aliquots of 12 μL of cell suspensions were transferred into 0.9 mm ID and 1.1 mm OD quartz capillary tubes (VitroCom, Boonton, NJ, USA, sample height of 25 mm) and sealed with Ch-SealTM tube sealing compound (Medex International, Inc., Burtonsville, MD, USA). Electron spin resonance (ESR) experiments were carried out at room temperature using an ESP300E spectrometer (Bruker BioSpin GmbH, Billerica, MA, USA), equipped with a standard rectangular mode TE102 cavity with following settings: microwave frequency ~ 9.38 GHz, microwave power 2 mW, sweep width 100 G, modulation frequency 100 kHz, modulation amplitude 0.5 G, receiver gain 2.4 × 10⁴, time constant 40.9 ms, conversion time 81 ms, and time per single scan 81 s. For each experimental point of ROS detection with CMH, two-scan field-swept ESR spectra were recorded. Intracellular CMH-related signal concentrations were determined using the following calculation: $C_{CMH} = C_{TEMPOL(1\text{ mM})} \times I_{CMH(t)} / I_{TEMPOL(1\text{ mM})}$ where C_{CMH} is the molar concentration of the oxidized form of CMH after incubation in cells, TEMPOL (1 mM) is 1 mM concentration of TEMPOL reference sample, $I_{TEMPOL(1\text{ mM})}$ is the ESR signal intensity of TEMPOL reference sample, and $I_{CMH(t)}$ is the ESR signal intensity for the oxidized form of CMH after incubation. All spectra were collected by adopting the same protocol. Experimental data were analyzed using the ORIGINPRO 9 software. Statistical analysis was performed using unpaired *t*-test.

DCF method for detection of intracellular ROS

Measurements of intracellular ROS levels were performed using 2',7'-dichlorodihydrofluorescein diacetate (DCFH₂-DA). Cells were incubated in the presence of 10 μM DCFH₂-DA in phosphate-buffered saline (PBS) at 37 °C for 30 min then washed two times with. The trapped fluorescent dye (DCF) inside the cells used to evaluate and detect intracellular ROS. The fluorescence values at different conditions were monitored by excitation at 498 nm and

emission 530 nm. Rotenone was used as a positive control at a concentration of 1 μM .

Mitochondrial membrane potential

Mitochondrial membrane potential in NIH3T3 mutated cells was determined using Tetramethylrhodamine, Methyl Ester, Perchlorate (TMRM, accumulating in the highly negatively charged interior of mitochondria) (Invitrogen, Carlsbad, CA, USA). Cell lines were seeded in 96-well plates (5000 cells/well) and treated with 50 nM tepotinib for 8 h. Cells were washed with PBS and suspended in PBS with 10 nM TMRM. Cells were incubated for 30 min at 37 °C. After, cells were washed with PBS and fluorescence was measured at excitation and emission wavelengths of 488 and 570 nm, respectively, with an Infinite 200 plate reader (Tecan Group Ltd.). Valinomycin was used as a control for loss of potential at a concentration of 1 μM .

Statistical analysis

Statistics and graphical presentation of the data except metabolomics data were performed using PRISM GRAPH (version 5.03). Data for each treatment group were represented as means \pm SD, if not written otherwise, as indicated and compared to evaluate significance using the Student *t*-test.

Acknowledgements

We thank PD Dr Andrzej Sienkiewicz (EPFL, Lausanne, Switzerland) for enabling ROS measurements at the Laboratory of Nanostructures and Novel Electronic Materials (EPFL, Lausanne, Switzerland) and Dr Aurélie Quintin (Inselspital Bern, Switzerland) for excellent technical assistance. This study was supported by Bernische Krebsliga, Stiftung zur Krebsbekämpfung and The Werner und Hedy Berger-Janser – Stiftung zur Erforschung der Krebskrankheiten (grants to MM).

Conflict of interest

The authors declare no conflict of interest.

Author contributions

MM and YZ designed the study; MP, AF, and KP performed the experiments. NZ performed metabolomics measurements and metabolomics data analysis. MP, AF, KP, JMN, YZ, MM, and NZ analyzed and interpreted data. MP and MM wrote the manuscript. NZ, JMN, DMA, YZ, and MM provided

resources. All authors read and approved the final manuscript.

References

- Goldberg ID & Rosen EM (1993) Hepatocyte growth factor-scatter factor (HGF-SF) and the c-met receptor. Introduction. *EXS* **65**, xiii–xv.
- Wang R, Ferrell LD, Faouzi S, Maher JJ & Bishop JM (2001) Activation of the Met receptor by cell attachment induces and sustains hepatocellular carcinomas in transgenic mice. *J Cell Biol* **153**, 1023–1034.
- Zeng ZS, Weiser MR, Kuntz E, Chen CT, Khan SA, Forslund A, Nash GM, Gimbel M, Yamaguchi Y, Culliford AT *et al.* (2008) c-Met gene amplification is associated with advanced stage colorectal cancer and liver metastases. *Cancer Lett* **265**, 258–269.
- Smyth EC, Sclafani F & Cunningham D (2014) Emerging molecular targets in oncology: clinical potential of MET/hepatocyte growth-factor inhibitors. *Onco Targets Ther* **7**, 1001–1014.
- Finisguerra V, Prenen H & Mazzone M (2016) Preclinical and clinical evaluation of MET functions in cancer cells and in the tumor stroma. *Oncogene* **35**, 5457–5467.
- Garber K (2014) MET inhibitors start on road to recovery. *Nat Rev Drug Discovery* **13**, 563–565.
- Beger RD (2013) A review of applications of metabolomics in cancer. *Metabolites* **3**, 552–574.
- Callejon-Leblic B, Garcia-Barrera T, Gravalos-Guzman J, Pereira-Vega A & Gomez-Ariza JL (2016) Metabolic profiling of potential lung cancer biomarkers using bronchoalveolar lavage fluid and the integrated direct infusion/gas chromatography mass spectrometry platform. *J Proteomics* **145**, 197–206.
- Liu X, Lu Y, Guan X, Dong B, Chavan H, Wang J, Zhang Y, Krishnamurthy P & Li F (2015) Metabolomics reveals the formation of aldehydes and iminium in gefitinib metabolism. *Biochem Pharmacol* **97**, 111–121.
- Merz AL & Serkova NJ (2009) Use of nuclear magnetic resonance-based metabolomics in detecting drug resistance in cancer. *Biomark Med* **3**, 289–306.
- Pavlova NN & Thompson CB (2016) The emerging hallmarks of cancer metabolism. *Cell Metab* **23**, 27–47.
- Bello-Fernandez C & Cleveland JL (1992) c-myc transactivates the ornithine decarboxylase gene. *Curr Top Microbiol Immunol* **182**, 445–452.
- Semenza GL (2010) HIF-1: upstream and downstream of cancer metabolism. *Curr Opin Genet Dev* **20**, 51–56.
- Serizawa M, Kusuhara M, Zangiocomi V, Urakami K, Watanabe M, Takahashi T, Yamaguchi K, Yamamoto N & Koh Y (2014) Identification of metabolic signatures associated with erlotinib resistance of non-

- small cell lung cancer cells. *Anticancer Res* **34**, 2779–2787.
- 15 Lui VW, Wong EY, Ho K, Ng PK, Lau CP, Tsui SK, Tsang CM, Tsao SW, Cheng SH, Ng MH *et al.* (2011) Inhibition of c-Met downregulates TIGAR expression and reduces NADPH production leading to cell death. *Oncogene* **30**, 1127–1134.
- 16 Bradley CA, Salto-Tellez M, Laurent-Puig P, Bardelli A, Rolfo C, Tabernero J, Khawaja HA, Lawler M, Johnston PG, Van Schaeybroeck S *et al.* (2017) Targeting c-MET in gastrointestinal tumours: rationale, opportunities and challenges. *Nat Rev Clin Oncol* **14**, 562–576.
- 17 Han P, Li H, Jiang X, Zhai B, Tan G, Zhao D, Qiao H, Liu B, Jiang H & Sun X (2017) Dual inhibition of Akt and c-Met as a second-line therapy following acquired resistance to sorafenib in hepatocellular carcinoma cells. *Mol Oncol* **11**, 320–334.
- 18 Medova M, Pochon B, Streit B, Blank-Liss W, Francica P, Stroka D, Keogh A, Aebersold DM, Blaukat A, Bladt F *et al.* (2013) The novel ATP-competitive inhibitor of the MET hepatocyte growth factor receptor EMD1214063 displays inhibitory activity against selected MET-mutated variants. *Mol Cancer Ther* **12**, 2415–2424.
- 19 Berthou S, Aebersold DM, Schmidt LS, Stroka D, Heigl C, Streit B, Stalder D, Gruber G, Liang C, Howlett AR *et al.* (2004) The Met kinase inhibitor SU11274 exhibits a selective inhibition pattern toward different receptor mutated variants. *Oncogene* **23**, 5387–5393.
- 20 Jeffers M, Schmidt L, Nakaigawa N, Webb CP, Weirich G, Kishida T, Zbar B & Vande Woude GF (1997) Activating mutations for the met tyrosine kinase receptor in human cancer. *Proc Natl Acad Sci USA* **94**, 11445–11450.
- 21 Giordano S, Maffe A, Williams TA, Artigiani S, Gual P, Bardelli A, Basilico C, Michieli P & Comoglio PM (2000) Different point mutations in the met oncogene elicit distinct biological properties. *FASEB J* **14**, 399–406.
- 22 Graveel C, Su Y, Koeman J, Wang LM, Tessarollo L, Fiscella M, Birchmeier C, Swiatek P, Bronson R & Vande Woude G (2004) Activating Met mutations produce unique tumor profiles in mice with selective duplication of the mutant allele. *Proc Natl Acad Sci USA* **101**, 17198–17203.
- 23 Medova M, Aebersold DM, Blank-Liss W, Streit B, Medo M, Aebi S & Zimmer Y (2010) MET inhibition results in DNA breaks and synergistically sensitizes tumor cells to DNA-damaging agents potentially by breaching a damage-induced checkpoint arrest. *Genes Cancer* **1**, 1053–1062.
- 24 Jastroch M, Divakaruni AS, Mookerjee S, Treberg JR & Brand MD (2010) Mitochondrial proton and electron leaks. *Essays Biochem* **47**, 53–67.
- 25 Divakaruni AS, Paradyse A, Ferrick DA, Murphy AN & Jastroch M (2014) Analysis and interpretation of microplate-based oxygen consumption and pH data. *Methods Enzymol* **547**, 309–354.
- 26 Scaini G, Rochi N, Benedet J, Ferreira GK, Teodorak BP, Comim CM, Constantino Lde S, Vuolo F, Constantino LC, Quevedo J *et al.* (2011) Inhibition of brain citrate synthase activity in an animal model of sepsis. *Rev Bras Ter Intensiva* **23**, 158–163.
- 27 Murphy MP (2009) How mitochondria produce reactive oxygen species. *Biochem J* **417**, 1–13.
- 28 Friese-Hamim M, Bladt F, Locatelli G, Stammberger U & Blaukat A (2017) The selective c-Met inhibitor tepotinib can overcome epidermal growth factor receptor inhibitor resistance mediated by aberrant c-Met activation in NSCLC models. *Am J Cancer Res* **7**, 962–972.
- 29 Depeint F, Bruce WR, Shangari N, Mehta R & O'Brien PJ (2006) Mitochondrial function and toxicity: role of B vitamins on the one-carbon transfer pathways. *Chem Biol Interact* **163**, 113–132.
- 30 Martinez-Reyes I, Diebold LP, Kong H, Schieber M, Huang H, Hensley CT, Mehta MM, Wang T, Santos JH, Woychik R *et al.* (2016) TCA cycle and mitochondrial membrane potential are necessary for diverse biological functions. *Mol Cell* **61**, 199–209.
- 31 Hui S, Ghergurovich JM, Morscher RJ, Jang C, Teng X, Lu W, Esparza LA, Reya T, Le Z, Yanxiang Guo J *et al.* (2017) Glucose feeds the TCA cycle via circulating lactate. *Nature* **551**, 115–118.
- 32 Faubert B, Li KY, Cai L, Hensley CT, Kim J, Zacharias LG, Yang C, Do QN, Doucette S, Burguete D *et al.* (2017) Lactate metabolism in human lung tumors. *Cell* **171**, 358–371 e9.
- 33 Fan J, Teng X, Liu L, Mattaini KR, Looper RE, Vander Heiden MG & Rabinowitz JD (2015) Human phosphoglycerate dehydrogenase produces the oncometabolite D-2-hydroxyglutarate. *ACS Chem Biol* **10**, 510–516.
- 34 Biczó G, Hegyi P, Dosa S, Shalbuyeva N, Berczi S, Sinervirta R, Hracsko Z, Siska A, Kukor Z, Jarmay K *et al.* (2011) The crucial role of early mitochondrial injury in L-lysine-induced acute pancreatitis. *Antioxid Redox Signal* **15**, 2669–2681.
- 35 Chen YJ, Mahieu NG, Huang X, Singh M, Crawford PA, Johnson SL, Gross RW, Schaefer J & Patti GJ (2016) Lactate metabolism is associated with mammalian mitochondria. *Nat Chem Biol* **12**, 937–943.
- 36 Lanning NJ, Castle JP, Singh SJ, Leon AN, Tovar EA, Sanghera A, MacKeigan JP, Filipp FV & Graveel CR (2017) Metabolic profiling of triple-negative breast cancer cells reveals metabolic vulnerabilities. *Cancer Metab* **5**, 6.
- 37 Chinopoulos C & Adam-Vizi V (2010) Mitochondria as ATP consumers in cellular pathology. *Biochem Biophys Acta* **1802**, 221–227.

- 38 Chen Y, Huang R, Ding J, Ji D, Song B, Yuan L, Chang H & Chen G (2015) Multiple myeloma acquires resistance to EGFR inhibitor via induction of pentose phosphate pathway. *Sci Rep* **5**, 9925.
- 39 Makinoshima H, Takita M, Matsumoto S, Yagishita A, Owada S, Esumi H & Tsuchihara K (2014) Epidermal growth factor receptor (EGFR) signaling regulates global metabolic pathways in EGFR-mutated lung adenocarcinoma. *J Biol Chem* **289**, 20813–20823.
- 40 Carloni S, Fabbri F, Brigliadori G, Ulivi P, Silvestrini R, Amadori D & Zoli W (2010) Tyrosine kinase inhibitors gefitinib, lapatinib and sorafenib induce rapid functional alterations in breast cancer cells. *Curr Cancer Drug Targets* **10**, 422–431.
- 41 Felser A, Lindinger PW, Schnell D, Kratschmar DV, Odermatt A, Mies S, Jenö P & Krahenbuhl S (2014) Hepatocellular toxicity of benzbromarone: effects on mitochondrial function and structure. *Toxicology* **324**, 136–146.
- 42 Arnould D (2007) Mitochondrial fragmentation in apoptosis. *Trends Cell Biol* **17**, 6–12.
- 43 Guo T, Zhu Y, Gan CS, Lee SS, Zhu J, Wang H, Li X, Christensen J, Huang S, Kon OL *et al.* (2010) Quantitative proteomics discloses MET expression in mitochondria as a direct target of MET kinase inhibitor in cancer cells. *Mol Cell Proteomics* **9**, 2629–2641.
- 44 Karbowski M & Youle RJ (2003) Dynamics of mitochondrial morphology in healthy cells and during apoptosis. *Cell Death Differ* **10**, 870–880.
- 45 Waring P (2005) Redox active calcium ion channels and cell death. *Arch Biochem Biophys* **434**, 33–42.
- 46 Sabharwal SS & Schumacker PT (2014) Mitochondrial ROS in cancer: initiators, amplifiers or an Achilles' heel? *Nat Rev Cancer* **14**, 709–721.
- 47 Cesi G, Walbrecq G, Zimmer A, Kreis S & Haan C (2017) ROS production induced by BRAF inhibitor treatment rewires metabolic processes affecting cell growth of melanoma cells. *Mol Cancer* **16**, 102.
- 48 Trachootham D, Lu W, Ogasawara MA, Nilsa RD & Huang P (2008) Redox regulation of cell survival. *Antioxid Redox Signal* **10**, 1343–1374.
- 49 Brookes PS (2005) Mitochondrial H(+) leak and ROS generation: an odd couple. *Free Radic Biol Med* **38**, 12–23.
- 50 Kubicek CP & Rohr M (1980) Regulation of citrate synthase from the citric acid-accumulating fungus, *Aspergillus niger*. *Biochim Biophys Acta* **615**, 449–457.
- 51 Currie E, Schulze A, Zechner R, Walther TC & Farese RV Jr (2013) Cellular fatty acid metabolism and cancer. *Cell Metab* **18**, 153–161.
- 52 Chen L, Liu T, Zhou J, Wang Y, Wang X, Di W & Zhang S (2014) Citrate synthase expression affects tumor phenotype and drug resistance in human ovarian carcinoma. *PLoS ONE* **9**, e115708.
- 53 Sharma AB, Sun J, Howard LL, Williams AG Jr & Mallet RT (2007) Oxidative stress reversibly inactivates myocardial enzymes during cardiac arrest. *Am J Physiol Heart Circ Physiol* **292**, H198–H206.
- 54 Freitas JJ, Pompeia C, Miyasaka CK & Curi R (2001) Walker-256 tumor growth causes oxidative stress in rat brain. *J Neurochem* **77**, 655–663.
- 55 Kaufmann P, Torok M, Hanni A, Roberts P, Gasser R & Krahenbuhl S (2005) Mechanisms of benzarone and benzbromarone-induced hepatic toxicity. *Hepatology* **41**, 925–935.
- 56 Paech F, Bouitbir J & Krahenbuhl S (2017) Hepatocellular toxicity associated with tyrosine kinase inhibitors: mitochondrial damage and inhibition of glycolysis. *Front Pharmacol* **8**, 367.
- 57 Lebedzinska M, Karkucinska-Wieckowska A, Giorgi C, Karczmarewicz E, Pronicka E, Pinton P, Duszyński J, Pronicki M & Wieckowski MR (2010) Oxidative stress-dependent p66Shc phosphorylation in skin fibroblasts of children with mitochondrial disorders. *Biochem Biophys Acta* **1797**, 952–960.
- 58 Kim WH, Park WB, Gao B & Jung MH (2004) Critical role of reactive oxygen species and mitochondrial membrane potential in Korean mistletoe lectin-induced apoptosis in human hepatocarcinoma cells. *Mol Pharmacol* **66**, 1383–1396.
- 59 Fuhrer T, Heer D, Begemann B & Zamboni N (2011) High-throughput, accurate mass metabolome profiling of cellular extracts by flow injection-time-of-flight mass spectrometry. *Anal Chem* **83**, 7074–7080.
- 60 Shepherd D & Garland PB (1969) The kinetic properties of citrate synthase from rat liver mitochondria. *Biochem J* **114**, 597–610.

Supporting information

Additional supporting information may be found online in the Supporting Information section at the end of the article.

Table S1. Up- or downregulated metabolite ions—comparison of unperturbed cell lines.

Table S2. Up- or downregulated metabolite ions in cell lines upon tepotinib treatment (0.5; 2; 8 h).